Rare earth element concentrations and Nd isotopes in the Southeast Pacific Ocean

C. Jeandel, H. Delattre, Mélanie Grenier, C. Pradoux, F. Lacan

Geochemistry Geophysics Geosystems G3

Article
Volume 14, Number XX
XX Month 2013
doi:10.1029/GC004309
ISSN: 1525-2027

Published by AGU and the Geochemical Society

Rare earth element concentrations and Nd isotopes in the Southeast Pacific Ocean

C. Jeandel
LEGOS (Université de Toulouse/CNRS/CNES/IRD), Observatoire Midi-Pyrénées, Toulouse, France

H. Delattre
LEGOS (Université de Toulouse/CNRS/CNES/IRD), Observatoire Midi-Pyrénées, Toulouse, France

Aix-Marseille Université, CNRS, IRD, CEREGE UM34, 13545 Aix-en-Provence, France

M. Grenier, C. Pradoux, and F. Lacan
LEGOS (Université de Toulouse/CNRS/CNES/IRD), Observatoire Midi-Pyrénées, Toulouse, France

[1] Three vertical profiles of rare earth element concentrations and Nd isotopic compositions have been measured in the remote southeast Pacific Ocean. The three stations represent contrasting environments: the oligotrophic center of the gyre (station GYR), the "transition zone" east of the South Tropical Front (station EGY), and the Peru-Chile upwelling marked by a pronounced oxygen minimum (station UPX). Rare earth concentrations display nutrient like vertical profiles except at UPX where surface waters are enriched. At this station Nd isotopic compositions are clearly more radiogenic than in the open ocean, suggesting that boundary exchange process is releasing lithogenic rare earth element from the volcanic Andes. Unexpected radiogenic values (ε_{Nd} reaching –3.7) are also observed at 2000 m at station GYR in the Upper Circumpolar Deep Water that commonly have ε_{Nd} values around –6. Exchange processes related to hydrothermal activity are suspected to produce this increase in ε_{Nd} in the vicinity of the East Pacific Rise. These results provide some guidance for higher resolution studies planned in this region by the international GEOTRACES program.

Components: 8700 words, 6 figures, 2 tables.

Keywords: Rare Earth Elements; Nd isotopes; marine geochemistry; Boundary Exchange; Ridge Exchange; Southeast Pacific.

Index Terms: 1040 Geochemistry: Radiogenic isotope geochemistry; 4808 Oceanography: Biological and Chemical: Chemical tracers; 4825 Oceanography: Biological and Chemical: Geochemistry.

Received 25 June 2012; **Revised** 1 November 2012; **Accepted** 20 November 2012; **Published** XX Month 2013.

Jeandel, C., H. Delattre, M. Grenier, C. Pradoux, and F. Lacan (2013), Rare earth element concentrations and Nd isotopes in the Southeast Pacific Ocean, *Geochem. Geophys. Geosyst.*, *14*, doi:10.1029/GC004309.

Theme: Oceanography

1. Introduction

[2] The oceanographic cruise BIOSOPE (December 2004, R/V *Atalante*, PI Hervé Claustre; [*Claustre et al*., 2008]) took place between Tahiti and Chile, crossing the South Pacific gyre along a northwest/southeast transect of about 8000 km (Figure 1a). This area is among the least studied of the world's oceans, notably for geochemical tracers. The BIOSOPE cruise track crosses various trophic and hydrological regimes of the South Pacific. Three stations were sampled (Figure 1a). The results provide preliminary data that hint to important processes that regulate the rare earth elements (REE) concentrations and the Nd isotopic composition in this remote area.

[3] The oceanic distributions of REE and the isotopic composition of neodymium are used as tracers of particulate scavenging processes and water mass transports [*Goldstein and Hemming*, 2003]. "Rare earth elements" design a group of 15 elements of atomic numbers ranging from 57 to 71. From La to Yb, the atomic mass increases while the size of the atom decreases, yielding fractionations between the different REE during geochemical processes. The REE fractionations relative to the continental source are identified by normalizing the measured REE concentrations to their respective average values in the Post-Archean Australian Sedimentary Shale (PAAS) [*McLennan*, 1989]. In seawater, several processes (e.g., adsorption, remineralization, scavenging, etc.) may cause fractionations within the group. The resulting dissolved PAAS-normalized REE patterns illustrate typical open-ocean features like heavy rare earth enrichment relative to the light ones and a depletion of cerium (Ce) relative to its neighboring REEs. The latter reveals the removal of this element often associated to particle scavenging and mostly Mn oxide formation [*Bertram and Elderfield*, 1993; *Bau et al*., 1996; *Tachikawa et al*., 1999a]. This depletion is expressed by the ratio Ce/Ce*, where Ce is the measured value and Ce* a theoretical concentration, calculated by interpolating its neighbor concentrations (equation given in Table 1 and Figure 4 captions [*Bertram and Elderfield*, 1993]). However, suboxic conditions could yield Mn oxide reduction and its release from the solid phase, and hence potentially liberate the retained Ce too [*Landing and Bruland*, 1987; *Moffet*, 1990; *Tachikawa et al*., 1999a]. Therefore, the "Ce anomaly" could be sensitive to the depleted oxygen conditions encountered within the oxygen minimum zone (OMZ).

[4] Among the REE, neodymium presents an additional interesting property due to its isotopic composition. The natural abundance of the stable ^{143}Nd radiogenic isotope varies as the result of the α-decay of its father the ^{147}Sm. This variation is expressed as ε_{Nd} and defined as follows:

$$\varepsilon_{Nd} = \left(\frac{\left(^{143}Nd/^{144}Nd\right)_{sample}}{\left(^{143}Nd/^{144}Nd\right)_{CHUR}} - 1 \right) * 10^4 \qquad (1)$$

where the measured ^{143}Nd/^{144}Nd atomic ratio of the sample is compared to the CHUR (CHondritic Uniform Reservoir) value of 0.512638, a reference for the average ^{143}Nd/^{144}Nd earth value [*Jacobsen and Wasserburg*, 1980].

[5] On the Earth's surface, ε_{Nd} values are varying from –56 to +13 according to the age and nature of the outcropping rocks and sediments [*Jeandel et al*., 2007]. The main sources of REE (and therefore Nd) to the oceans are lithogenic, and ε_{Nd} values increase along the thermohaline circulation, from an average of –13.1 in the North Atlantic Subpolar gyre, to –3.9 in the North Pacific [*Lacan et al*., 2012]. This distribution reflects a balance between the intensity and location of the Nd sources and its redistribution within the ocean by the particle/solution reversible exchange and the general circulation transport. It is today assumed (i) that the water masses acquire their ε_{Nd} values by exchange processes when flowing along continental margins but also (ii) that surface waters flowing below intense dust fluxes, off Saharan desert for example, might also be modified by atmospheric inputs [*Jeandel et al*., 1998; *Lacan and Jeandel*, 2005; *Arsouze etal*., 2007, 2009; *Jones et al*., 2008; *Siddall et al*., 2008; *Rempfer et al*., 2011; *Rickli et al*., 2011; *Carter et al*., 2012; *Grasse et al*., 2012]. Although the ratio between REE concentrations in hydrothermal vent fluids and seawater typically lies in the range of 6–100, several works showed that Fe-Mn oxide precipitates actively remove the seawater REE in the vicinity of the vents [*Michard et al*., 1983; *Piepgras and Wasserburg*, 1985, *German et al*., 1990]. Therefore, hydrothermal fluids are considered as a negligible source and even a sink for Nd oceanic budgets, and consequently neglected in the recent modeling of the Nd oceanic cycle [*Jones et al*., 2008; *Siddall et al*., 2008; *Arsouze et al*., 2009; *Rempfer et al*., 2011]. Far from any lithogenic input, ε_{Nd} has a conservative behavior in the ocean [*von Blanckenburg*, 1999], which allows using it as a circulation tracer [*Piepgras and Wasserburg*, 1987; *Jeandel*, 1993; *Carter et al*., 2012; *Grasse et al*., 2012; *Stichel et al*.,

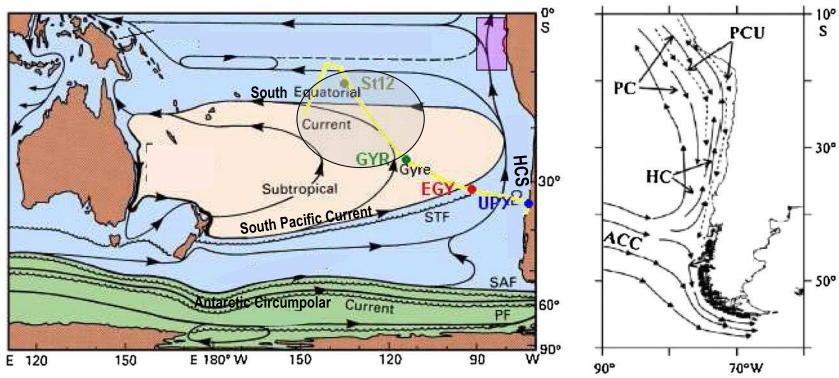

Figure 1. (a) BIOSOPE cruise track (in yellow) and station locations reported on the circulation scheme of the South Pacific Ocean, modified after *Tomczak and Godfrey* [2003]. Station UPX (72.49°W; 34.69°S); Station EGY (91.41°W; 31.90°S); Station GYR (113.99°W; 26.07°S). St 12 of the EqPac cruise is also reported [*Lacan and Jeandel*, 2001]. STF = SubTropical Front; SAF = SubAntarctic Front; PF = Polar Front, HCS = Humbolt Current System. South Equatorial Current (SEC), South Pacific Current (SPC), Antarctic Circumpolar Current (ACC) are described in the text. The shaded gray area locates the High Surface Evaporation Area (HSEA) and the purple one identified the region studied by *Grasse et al*. [2012]. (b) Details of the different currents composing the HCS along the Peru-Chile coast, modified after *Silva et al*. [2009]. HC = Humboldt Current; PC = Peru Countercurrent; PCU = Peru-Chile Undercurrent.

2012]. Finally, the budgets and mass fluxes that are calculated using Nd isotopes and REE concentrations could be very useful to constrain budgets of other elements [*Jeandel et al*., 2011].

[6] The first objective of this work is to improve the ε_{Nd} and REE database in this poorly studied region, which is of particular interest for characterizing the main pathways of water masses feeding the western Pacific [*Tomczak and Godfrey*, 2003]. The second objective is to determine whether the proximity to the Andes and the numerous hydrothermal vents of the very active East Pacific Rise [*Piepgras and Wasserburg*, 1985; *Klinkhammer and Hudson*, 1986] influence the South Pacific water neodymium signatures. Although only three stations of the BIOSOPE cruise were dedicated to the REE and Nd isotope measurements, they are representative of contrasting environments. Station UPX (72.49°W; 34.69°S) is located close to the Andean coast and characterized by high level of nutrients and chlorophyll associated with the Chile-Peru upwelling. It is directly influenced by cold waters that originate from the Antarctic Circumpolar Current and is marked by an intense oxygen minimum zone [*Claustre et al*., 2008]. On the edge of the southeast Pacific tropical gyre, the EGY station (91.41°W; 31.90°S) is located just east of the subtropical front corresponding to the "Transition Zone" described by *Tomczak and Godfrey* [2003]. Finally, station GYR (113°99°W; 26.07°S) is located close to the source of salty South Pacific tropical waters, which flow in the upper part of the thermocline and are formed by convective sinking of surface water through evaporation in the high surface evaporation area (HSEA, Figure 1a, [*Tsuchiya et al*., 1989; *Sokolov and Rintoul*, 2000; *Grenier et al*., 2013]. In addition, it is also located just above a very tectonically active region influenced at depth by hydrothermal inputs [*Klinkhammer and Hudson*, 1986; *Kingsley et al*., 2007]. Documenting REE and Nd parameters at this later station will help us to characterize water masses that are feeding the western and equatorial Pacific and evaluate the potential impact of hydrothermal vent fluids on the Nd signature of the local deep waters.

2. Dynamic and Hydrographic Context

2.1. Currents

[7] The water masses characterized in this study are transported by currents that are briefly described here. The general circulation of the southeast Pacific Ocean follows an anticyclonic subtropical gyre centered on 20°S (Figure 1a; [*Tomczak and Godfrey*, 2003]). Its northern branch flowing westward is mostly formed by the South Equatorial Current, which extends from 5°S to 25°S and flows over at least 1000 m. It transports various water masses from the surface down to the Antarctic Intermediate Water (AAIW), among them those observed at station GYR. The south limb of the gyre is formed by the South Pacific Current, which flows eastward around 30°S. When approaching South America, this current turns northward and flows parallel to

Table 1. REE Concentrations (pmol/kg) Measured at the Three Stations Together With the Hydrological Parameters. Ce Anomaly, Calculated as Ce/Ce* = $2[Ce]_n/([La]_n + [Pr]_n)$ is Also Reported, As Well As the Ratio Between Normalized La and Yb: (La/Yb)n

Station	Depth (m)	θ (°C)	Salinity	Oxygen (μmol/kg)	La	2σ	Ce	2σ	Pr	2σ	Nd	2σ	Sm	2σ	Eu	2σ	Gd	2σ	Tb	2σ	Dy	2σ	Ho	2σ	Er	2σ	Tm	2σ	Yb	2σ	Lu	2σ	(La/Yb)n	Ce/Ce*
UPX	15	12.64	34.34	177.26	31.6	0.7	39.6	0.8	6.1	0.1	26.6	0.6	5.8	0.1	1.2	0.0	6.1	0.2	0.9	0.0	6.1	0.2	1.5	0.0	4.8	0.1	0.6	0.0	4.0	0.1	0.7	0.0	0.5	0.6
	15	12.64	34.34	177.26	34.5	0.9	42.4	1.1	6.5	0.2	27.5	0.8	5.1	0.1	1.3	0.0	6.1	0.2	0.9	0.0	6.3	0.2	1.5	0.0	4.8	0.2	0.7	0.0	4.1	0.1	0.7	0.0	0.5	0.6
	100	11.36	34.588	34.094	17.8	0.3	13.6	0.2	2.8	0.0	11.6	0.2	2.1	0.0	0.5	0.0	3.1	0.1	0.5	0.0	3.5	0.1	0.9	0.0	3.2	0.1	0.5	0.0	2.8	0.1	0.5	0.0	0.4	0.4
	100	11.36	34.588	34.094	22.9	0.3	16.8	0.3	3.2	0.1	13.1	0.2	2.3	0.0	0.5	0.0	3.2	0.1	0.5	0.0	3.5	0.1	0.9	0.0	3.2	0.1	0.5	0.0	2.8	0.1	0.5	0.0	0.5	0.4
	250	9.87	34.6225	14.173	18.6	0.5	12.5	0.3	2.7	0.1	11.1	0.3	1.8	0.1	0.5	0.0	2.8	0.1	0.4	0.0	3.3	0.1	1.0	0.0	3.5	0.1	0.5	0.0	3.2	0.1	0.6	0.0	0.3	0.4
	250	9.87	34.6225	14.173	19.4	0.5	11.7	0.3	2.6	0.1	10.2	0.3	1.7	0.1	0.4	0.0	2.8	0.1	0.4	0.0	3.3	0.1	0.9	0.0	3.5	0.1	0.5	0.0	3.2	0.1	0.6	0.0	0.4	0.3
	300	9.28	34.5853	16.946	19.7	0.5	11.7	0.3	2.8	0.1	11.0	0.3	1.9	0.1	0.5	0.0	2.9	0.1	0.4	0.0	3.6	0.1	1.0	0.0	3.8	0.1	0.5	0.0	3.4	0.1	0.6	0.0	0.3	0.3
	400	8.12	34.5063	41.588	17.6	0.4	7.5	0.2	2.4	0.1	10.3	0.3	2.0	0.1	0.5	0.0	2.9	0.1	0.5	0.0	3.8	0.1	1.1	0.0	4.1	0.1	0.6	0.0	3.9	0.1	0.7	0.0	0.3	0.2
	800	4.66	34.3376	155.134	21.1	0.3	11.0	0.1	3.1	0.0	13.0	0.3	2.3	0.1	0.6	0.0	3.7	0.1	0.6	0.0	4.6	0.1	1.3	0.0	5.0	0.1	0.7	0.0	5.0	0.1	0.9	0.0	0.2	0.3
EGY	20	18.25	34.6624	231.15	7.6	0.1	6.6	0.1	1.1	0.0	4.0	0.1	0.5	0.0	0.1	0.0	1.0	0.0	0.2	0.0	1.3	0.0	0.4	0.0	1.2	0.0	0.1	0.0	0.6	0.0	0.1	0.0	0.7	0.5
	70	16.36	34.6494	242.682	8.3	0.2	8.5	0.2	1.1	0.0	4.0	0.1	0.4	0.0	0.1	0.0	0.9	0.0	0.1	0.0	1.1	0.0	0.3	0.0	1.2	0.0	0.1	0.0	0.6	0.0	0.1	0.0	0.8	0.6
	280	10.62	34.2218	210.905	11.3	0.3	5.4	0.1	1.5	0.0	6.3	0.2	4.4	0.1	0.3	0.0	1.8	0.1	0.3	0.0	2.5	0.1	0.7	0.0	2.5	0.1	0.3	0.0	1.8	0.1	0.3	0.0	0.4	0.3
	370	8.09	34.2956	171	20.5	0.5	12.3	0.3	2.8	0.1	10.0	0.3	1.6	0.1	0.4	0.0	2.7	0.1	0.4	0.0	3.6	0.1	1.1	0.0	4.0	0.1	0.6	0.0	3.6	0.1	0.6	0.0	0.3	0.3
	800	4.70	34.2715	207.924	15.9	0.4	3.6	0.1	2.2	0.1	9.8	0.3	1.7	0.1	0.5	0.0	3.1	0.1	0.5	0.0	4.3	0.1	1.2	0.0	4.8	0.1	0.7	0.0	4.7	0.2	0.9	0.0	0.2	0.1
	3200	1.50	34.6921	160.772	31.8	0.5	3.1	0.1	4.1	0.1	18.8	0.4	3.1	0.1	0.8	0.0	5.5	0.1	0.8	0.0	7.3	0.2	2.1	0.0	7.8	0.1	1.2	0.0	8.2	0.2	1.5	0.0	0.2	0.1
GYR	50	22.10	36.0255	211.529	3.3	0.1	1.7	0.0	0.6	0.0	2.8	0.1	0.5	0.0	0.1	0.0	1.0	0.1	0.2	0.0	1.3	0.1	0.4	0.0	1.3	0.0	0.1	0.0	0.7	0.0	0.1	0.0	0.3	0.3
	170	19.51	35.6123	208.854	3.2	0.1	1.3	0.0	0.6	0.0	2.7	0.1	0.6	0.0	0.1	0.0	1.0	0.0	0.2	0.0	1.3	0.1	0.4	0.0	1.3	0.0	0.2	0.0	0.7	0.0	0.1	0.0	0.3	0.2
	700	5.45	34.2918	213.149	14.0	0.3	2.4	0.1	1.9	0.1	8.8	0.2	1.6	0.1	0.4	0.0	2.8	0.1	0.4	0.0	4.0	0.1	1.2	0.0	4.5	0.1	0.7	0.0	4.5	0.1	0.8	0.0	0.2	0.1
	2000	1.92	34.64	150.446	27.9	0.7	3.5	0.1	3.1	0.1	14.6	0.4	2.6	0.1	0.6	0.0	4.6	0.1	0.7	0.0	6.1	0.2	1.8	0.0	7.0	0.2	1.1	0.0	7.4	0.3	1.4	0.0	0.2	0.1
	2975	1.67	34.6766	149.02	34.8	0.8	9.2	0.2	4.3	0.1	18.2	0.5	4.1	0.1	0.9	0.0	5.4	0.2	0.8	0.0	7.0	0.2	2.0	0.1	7.7	0.2	1.2	0.0	8.3	0.2	1.6	0.0	0.2	0.1

the Peru-Chile coast without any contact with it. Indeed, between the edge of the gyre and the Chile coast—where stations EGY and UPX are located—the Humboldt Current System (HCS) comprises all the currents found along the Peru-Chile coast (Figure 1b; [*Silva et al*., 2009]). The Humboldt Current (HC) represents the northern vein of the Antarctic Circumpolar Current (ACC) and transports cold surface Subantarctic Water toward the equator [*Silva et al*., 2009]. Other constituents of the HCS are the Peru Counter Current, which transports warmer and more salty subtropical water southward, and the Peru-Chile Undercurrent, which transports Equatorial SubSurface Water (ESSW) southward too and is characterized by a subsurface salinity maximum (Figure 1b; [*Silva et al*., 2009]). This coastal undercurrent, situated under the HC and restricted to a narrow band in the neighborhood of the slope break, flows between 10°S and 48°S [*Claustre et al*., 2008]. The Chile-Peru upwelling is the most important upwelling in the world's ocean and the most productive one. It extends from 40°S to the equator where it joins the equatorial upwelling [*Tomczak and Godfrey*, 2003].

2.2. Water Masses

[8] In the southeast Pacific Ocean, the circulation of the deepest water masses (>1000 m depth) is essentially meridian. *Kawabe and Fujio* [2010] suggest that waters found at 2000 m and 3000 m at station GYR and EGY are Upper Circumpolar Deep Waters (UCDW, $34.64 < S < 34.69$, $1.5°C < T < 1.9°C$ in Figure 2a, also displaying low oxygen content of 150 to 160 μmol/kg in Figure 2b). Originating from the Southern Ocean, they flow northward in the studied area and then northwestward across the South Pacific Basin [*Kawabe and Fujio*, 2010; *Grenier et al*., 2013]. This scheme is consistent with the general geostrophic circulation [*Reid*, 1997]. AAIW is formed north of the Polar Front, mostly off southwest America [*England et al*., 1993]. It flows between 1000 and 800 m and is observed at the three stations studied here (Figure 2). It is characterized by an oxygen maximum, a low salinity (~34.3), and a temperature around 3°C. East of 90°W, another intermediate water mass occurs, fresher ($34 < S < 34.4$) and warmer ($11°C < T < 13°C$) than the AAIW: the Eastern South Pacific Intermediate Water (ESPIW) that subducts off the Chilean coast and spreads from 50 to 500 m between 20°S and 38°S [*Schneider et al*., 2003]. ESPIW is mostly observed at station EGY (Figure 2).

[9] Water masses with contrasting properties are encountered in the thermoclines of the studied area. The Eastern South Pacific Central Water (ESPCW) flows above 500 m and is observed at station GYR (Figure 2). East of 110°W, the Subantarctic Surface Water is advected, reducing the salinity of the thermocline of the Peru/Chile Current. *Tomczak and Godfrey* [2003] named these waters "transition waters" (TrW), here observed in the EGY and UPX thermoclines. Finally, the ESSW flows between 150 and 300 m depth along the Chilean coast. It has been observed at station UPX, characterized by a high salinity and a low oxygen content that extends from 50 to 450 m depth. The OMZ is dropping down to values lower than 15 μmol/kg at 250 m as shown in Figure 2b [*Schneider et al*., 2003]. The OMZ is still visible at station EGY, although values do not fall below 170 μmol/kg (at 370 m) and almost vanishes at station GYR, where it deepens slightly.

3. Material and Methods

[10] Samples were collected with a conductivity-temperature-depth rosette equipped with Niskin bottles that have been proven to be reliable for Nd and REE clean collection by the GEOTRACES intercalibration exercise [*van de Flierdt et al*., 2012]. Nonfiltered seawater (10 L) was directly acidified onboard using Suprapur^R HCl and stored. Although it has been shown before at open ocean locations that Nd isotopic composition of different fractions (unfiltered seawater, the "dissolved" fraction (<0.45 or 0.2 μm), the truly dissolved and colloidal ones) give the same ε_{Nd} values within error [*Dahlqvist et al*., 2005], this cannot be assumed to be valid in general. Here the water samples have not been filtered, which prevents any direct comparison to dissolved Nd data and yields us to interpret our results cautiously, especially close to the coast and the hydrothermal vent, where particles might influence the Nd parameter signatures.

3.1. Rare Earth Element Concentrations

[11] Back to the land-based laboratory (LEGOS, Observatoire Midi-Pyrénées, Toulouse, France, http://www.legos.obs-mip.fr/recherches/equipes/geomar), aliquots of 500 mL were taken from these 10 L samples for REE concentration measurements. To each aliquot, a spike solution artificially enriched in ^{150}Nd (97.84%) and ^{172}Yb (94.9%) was added. After a 3 day equilibration period, purified $FeCl_3$ diluted in 0.1 M HCl was added. The pH was then increased to 7–8 by addition of NH_4OH, yielding an

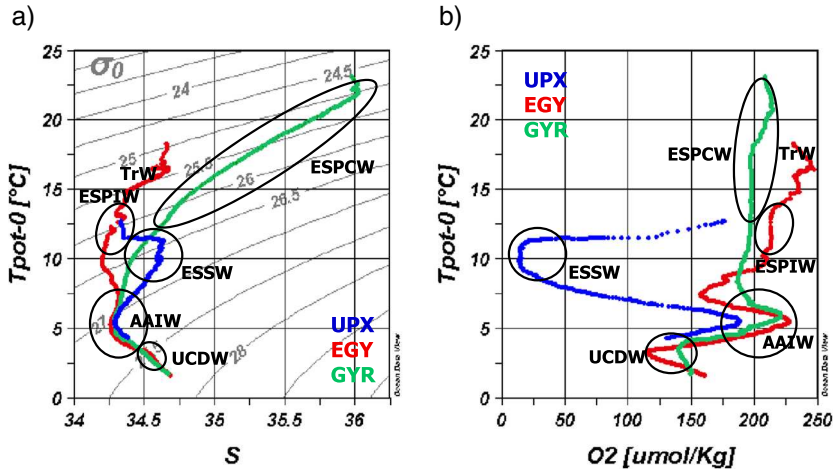

Figure 2. Potential temperature-salinity (Figure 2a) and temperature-oxygen (Figure 2b) diagrams of the studied stations, which allow identifying the following water masses: Eastern South Pacific Central Water (ESPCW), Eastern South Pacific Intermediate Water (ESPIW), Transition Water (TrW), Equatorial SubSurface Water (ESSW), Antarctic Intermediate Water (AAIW) and Upper Circumpolar Deep Water (UCDW), whose characteristics are discussed in the text.

extraction of the REE by iron oxide coprecipitation. After several centrifugation steps and supernatant removal, the precipitate was dissolved in 1 mL 6 M HCl and loaded on an anion exchange column packed with 2 mL of AG1X8 resin. REE were eluted with 4 mL 6 M HCl. This solution was evaporated and the residue redissolved in 0.4 mL 0.32 M HNO_3. Concentrations were measured using an inductively coupled plasma-mass spectrometer (ICPMS, Agilent 7500). The added ^{150}Nd and ^{172}Yb spikes enabled using isotopic dilution to calculate the concentrations of these two REE. All the REE concentrations have also been determined by external calibration, using indium and rhenium as internal standards to control any sensitivity drift of the spectrometer. Comparing Nd and Yb concentrations deduced from the external calibration to their values derived from isotopic dilution provides the recovery of the whole chemical extraction. Corrections for this recovery are then applied to the other REE [*Lacan and Jeandel*, 2001]. Average blank values ($n = 3$) represented less than 3% of the signal for La and Ce, 1% for the MREE (Pr to Gd), and less than 0.1% for the remaining REE. The detection limit (three times the average blank values) was 0.04×10^{-12} mol/L of seawater for Nd for example. Our measurements were characterized by a precision on Nd concentration of 10%, both with a 95% confidence interval (2σ). Because of isobaric interferences on europium and samarium masses (20 to 30%) from barium and cerium oxides, our middle REE results will have to be considered cautiously. Three samples were duplicated at station UPX (15, 100, and 250 m) and results are consistent within less than 10% for Nd for example (Table 1), assessing the external reproducibility of our data.

3.2. Nd Isotopic Composition

[12] After increasing the pH to 3.4–3.7 by addition of Suprapur® NH_4OH, each 10 L sample was loaded on two C18 SepPak cartridges (one cartridge per 5 L) previously loaded with a REE complexant (HDEHP/H_2MEHP) that quantitatively extracts REE from seawater [*Shabani et al.*, 1992]. REE were then eluted using distilled 6 M HCl, dried and then dissolved again in 1.5 mL 1 M HCl. This solution was loaded on a cationic exchange column packed with a resin Biorad AG50W-X8 (200–400 mesh) and rinsed with several different acids to remove the matrix before REE elution with 6 mL 6 M HCl. The final Nd extraction was conducted in 0.2 M HCl using an anionic exchange column packed with 0.5 mL of Ln-Spec resin [*Tachikawa et al.*, 1999a]. For samples containing more than 9 ng of Nd, Nd isotopic composition was determined by thermal ionization mass spectrometry in static mode (TIMS, ThermoFinnigan MAT 261, Observatoire Midi-Pyrénées, Toulouse). Remaining ε_{Nd} analyses (5 samples, Table 2) were performed at the University of Bristol, on a ThermoFinnigan Neptune MC/ICPMS, fitted with 9 Faraday collectors with 10^{11} Ω resistors and operated with low resolution slits. Whatever the mass spectrometer, mass fractionation was corrected using a $^{146}Nd/^{144}Nd$ ratio of 0.7219. However, as underlined by *Vance and Thirlwall* [2002], MC/ICPMS generates a residual instrumental mass discrimination that has to

be corrected using a double normalization based on correlations between $^{146}Nd/^{144}Nd$, normalized $^{143}Nd/^{144}Nd$, and $^{142}Nd/^{144}Nd$. To monitor instrumental drift, 15 analysis of La Jolla standard were performed with TIMS and gave 0.511886 ± 0.000020 (2σ). The generally accepted value being 0.511860 ± 0.000020 (2σ), we corrected all the measurements from a machine bias of 0.000026. On the Neptune, 20 analysis of La Jolla standard bracketed multiples of eight samples and gave an average value of 0.511879 ± 0.000005 (2σ). Thus, we corrected all the measurements from a machine bias of 0.000019. As part of the recent GEOTRACES intercalibration [*van de Flierdt et al.*, 2012], Bristol and Toulouse teams measured ε_{Nd} values comparable within 0.3 ε units on the same surface and deep seawater samples, which validates the present data set. However, despite the good internal precisions of both machines, ε_{Nd} data reported in Table 2 are often affected by relatively large error bars. This reflects the fact that the sample amounts analyzed were often at the limits of each machine (down to 3 ng on the MC/ICPMS and 9 ng on the TIMS). Blanks of the chemical procedure for Nd isotopic measurements represent less than 1% of the signal. The three samples duplicated at UPX gave consistent ε_{Nd} values within the error bars (Table 2).

4. Results

4.1. REE Concentrations

[13] Results of the REE concentration analyses are presented in Table 1, the Nd vertical profiles are shown in Figure 3 and all the REE patterns obtained after normalizing the REE data to an average shale reference (PAAS) are depicted in Figure 4. At station GYR and EGY, the Nd vertical profiles show depleted values at the surface (2.8 to 4 pmol/kg) and an increase with depth, reaching more than 18 pmol/kg at 3200 m at EGY. Although these deep concentrations are low compared to the remaining Pacific deep waters [*Lacan et al.*, 2012], this "nutrient-like" shape is consistent with the REE behavior generally observed in the open ocean [*Bertram and Elderfield*, 1993; *Tachikawa et al.*, 1999a]. Contrastingly, the REE vertical distributions at station UPX —illustrated by the Nd profile, but also observed for the other REE and reported in Table 1— present an inverse shape compared to those at EGY and GYR (Figure 3). A sharp decrease of the Nd concentration is observed at this station, from ~27 pmol/kg near the surface to ~10.5 pmol/kg at 250 m, value comparable to those observed at GYR and EGY for the same depth.

[14] The REE patterns show a systematic enhancement of the Ce anomaly with depth together with a decrease of the $(La/Yb)_N$ ratio as shown in Figure 4. Again, these variations are consistent with the oceanic REE behaviors, characterized by the poor solubility of Ce compared to the other REE and the higher solubility of the heavy REE compared to the light ones resulting in an evolution of the $(La/Yb)_N$ with depth [*Bertram and Elderfield*, 1993; *Tachikawa et al.*, 1999b]. The vertical gradients of these two parameters are decreasing from coast to open ocean (UPX to GYR), as illustrated in Figures 4b and 4c.

4.2. Nd Isotopes

[15] Nd isotopic compositions (represented as ε_{Nd}) are reported in Table 2 and Figure 5. On average, Nd isotopic compositions are more radiogenic at station UPX than at the two others. Surface waters of station UPX show positive ε_{Nd} values (0.3 ± 0.6); they decrease to -4.5 ± 0.5 at around 250–300 m depth and reach -5.5 ± 0.5 at 800 m. At station EGY, all the values are between –6 and –7, except for the more radiogenic value of -4 ± 0.5 measured at 370 m. At station GYR the ε_{Nd} values decrease from -2.7 ± 0.4 at the surface to -6.9 ± 0.5 at 700 m depth. Surprisingly, the value rises to -3.7 ± 0.7 at 2000 m before decreasing again down to -5.2 ± 0.4 in the deepest waters (2975 m).

5. Discussion

5.1. Boundary Exchange

[16] Only surface and intermediate waters could be collected in the shallow and coastal station UPX (~60 km from the coast). The radiogenic Nd isotopic composition in uppermost waters (15 m) together with their high REE contents displaying flat patterns indicate that these waters are receiving lithogenic inputs (Figures 3, 4, and 5). Figure 6 displays ε_{Nd} data of rocks and sediments extracted from the geochemical data set EarthChem (http://www.earthchem.org). The distribution of ε_{Nd} values of the outcropping rocks and sediments along the Chile coast confirms that the lithogenic source is characterized by values ranging from 0 to +5. Because the samples were not filtered, we cannot exclude that part of the observed high REE content is due to the occurrence of suspended particles in the sample. Two pathways could bring this lithogenic material into coastal waters: wind-driven erosion or/and remobilization of shelf sediments deposited by the river discharges. At 35°S, winds

Table 2. Results of the ε_{Nd} Values Measured at the Three Stations[a]

Station	Depth (m)	Duplicate Name	θ (°C)	Salinity (psu)	Oxygen (μmol/kg)	Water Mass	ε_{Nd}	2σ
UPX	15	B1	12.64	34.34	177.26	surface water	0.7	0.4
	15	B2	12.64	34.34	177.26	surface water	−0.2	0.6
	100	B3	11.36	34.59	34.09	ESPIW	−1.5	0.6
	100	B4	11.36	34.59	34.09	ESPIW	−0.9	0.6
	250	B5	9.87	34.62	14.17	ESSW	−5.0	0.5
	250	B6	9.87	34.62	14.17	ESSW	−4.4	0.4
	300	B7	9.28	34.59	16.95	ESSW	−4.0	0.5
	400	B8	8.12	34.51	41.59	ESSW	-	-
	800	B10	4.66	34.34	155.13	AAIW	−5.5	0.5
EGY	**20***	#20	18.25	34.66	231.15	TrW	−6.4	0.3
	70*	#70	16.36	34.65	242.68	TrW	−6.0	0.3
	280*	#280	10.62	34.22	210.91	TrW	−7.1	0.2
	370	#370	8.09	34.30	171.00	ESPIW	−4.0	0.5
	800	#800	4.70	34.27	207.92	AAIW	−6.5	0.5
	3200	#3200	1.50	34.69	160.77	UCDW	−6.8	0.8
GYR	**50***	#17	22.10	36.03	211.53	ESPCW	−2.7	0.4
	170*	#13	19.51	35.61	208.85	ESPCW	−3.1	0.5
	700	#12	5.45	34.29	213.15	AAIW	−6.9	0.5
	2000	#6	1.92	34.64	150.45	UCDW	−3.7	0.7
	2975	#1	1.67	34.68	149.02	UCDW	−5.2	0.4

[a]Hydrographic parameters are recalled. The five samples analyzed by MC/ICPMS are in bold and marked with an asterisk.

are blowing from the west (ocean side) all over the year, turning north very close to the coast where they are forcing the upwelling [*Tomczak and Godfrey*, 2003]. In addition, the abundant rainfall on the coast prevents any desert development, contrasting to the north of Chile [*Schneider et al*., 2003]. Both arguments are not arguing in favor of a dust input in the studied area. We therefore suggest that the main source is resuspension and/or release of dissolved Nd from shelf sediments, in agreement with previous results in other regions [*Jeandel et al*., 1998; *Lacan and Jeandel*, 2001; 2005; *Rickli et al*., 2011; *Carter et al*., 2012; *Grasse et al*., 2012; *Grenier et al.*, 2013]. Subsurface (ESPIW) and intermediate (AAIW) waters are also more radiogenic at UPX than at the two other stations, without showing a clear Nd concentration enrichment. This leads us to assume that these water masses changed their isotopic composition at the contact of the margin following a "Boundary Exchange" process as described by *Lacan and Jeandel* [2001, 2005] and modeled by *Arsouze et al*. [2009] and *Rempfer et al*. [2011]. However, comparison of Arsouze's model simulations to our results shows that the model estimated surface ε_{Nd} values higher (by 2 to 3 units) than the measured ones, although the vertical decreasing gradient was correctly reproduced. This model overestimation could reflect either an exaggeration of the simulated Boundary Exchange process or an underestimate of the coastal currents, due to the 2° by 2° grid of the circulation model. Because Ce scavenging is mostly driven by the formation of Mn oxides on the settling particles [*Bau et al*., 1996; *Tachikawa et al*., 1999a; *Akagi et al*., 2011], it was expected that Ce could be released together with Mn in suboxic environments. Our data did not allow confirming such behavior: although six REE patterns have been determined within the OMZ, which extends from 50 to 450 m at station UPX, no real tendency toward a decrease of the Ce anomaly at these depths has been detected. This could indicate that adsorption processes involve particulate phases other than Mn oxides. Because our samples are not filtered, the other possibility is that dissolution takes place but does not affect their total Ce balance (dissolved + particles).

5.2. Water Mass ε_{Nd} Fingerprint

[17] At station EGY, ε_{Nd} values of surface and intermediate waters are relatively negative and homogeneous with depth, except at 370 m. This station is located in the "Transition Zone" [*Tomczak and Godfrey,* 2003] marked by cold thermocline waters originating from the Southern Ocean. *Carter et al*. [2012] provided data in the upper layers of the southeast Pacific sector of the ACC. Their station 22 (60°32′ S; 108°18′ W) identified that ACC surface and subsurface waters are labeled with ε_{Nd} values of -7.7 ± 0.3. Following the general circulation scheme [*Tomczak and Godfrey*, 2003], these

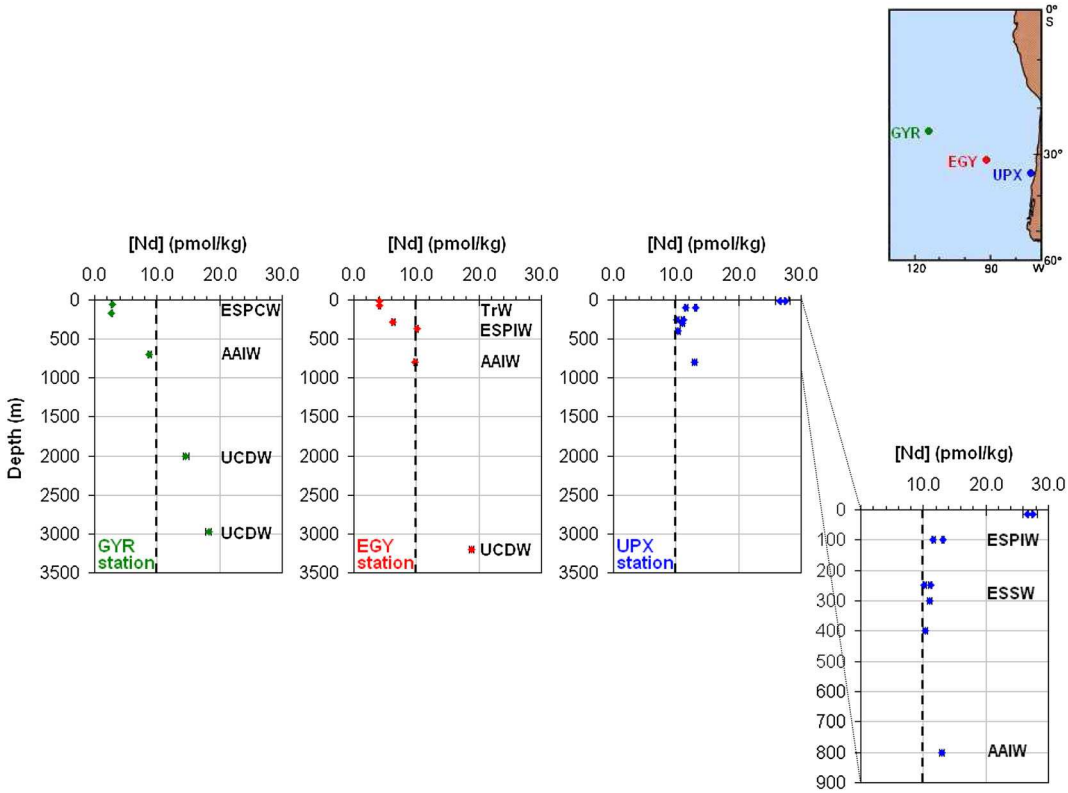

Figure 3. Vertical profiles of the Nd concentrations at the station GYR, EGY and UPX. An extended scale for the upper layers of station UPX is proposed. The dotted line marks the Nd concentration of 10 pmol/kg. Acronyms recall the water mass names.

waters are potentially sources of the thermocline waters found at EGY, displaying consistent — although slightly more radiogenic — ε_{Nd} values of –6 to –7. The surprising higher value at 370 m (–4.0 ± 0.5) corresponds to the ESPIW, a water mass that forms through the process of subduction off the Chile coast between 33°S and 38°S [*Schneider et al*., 2003]. Therefore, ESPIW likely transports properties acquired at the surface and subsurface off the coastal Chile. The radiogenic ε_{Nd} values found at UPX at 15 m and within the OMZ are consistent with the ESPIW Nd signature found at EGY and therefore this formation scheme. This confirms the ability of the ε_{Nd} tracer to fingerprint the water masses, as soon as they leave the closest contact with lithogenic sources, in agreement with modeling results [*Arsouze et al*., 2009; *Rempfer et al*., 2011].

[18] The isotopic signatures measured at stations EGY and GYR for the AAIW are –6.5 ± 0.5 and –6.9 ± 0.5, respectively. These data are consistent with that of *Grasse et al*. [2012], who found an ε_{Nd} value of –7 for AAIW at their station #103, suspected to be influenced by the subtropical gyre circulation. However, they are slightly more radiogenic than the value of –8 ± 0.3 observed at 12°S to 140°W for the same water mass [*Lacan and Jeandel*, 2001]. A possible explanation is that the AAIW measured at 12°S followed a trajectory that bypassed the possible influence of Andean inputs as observed here.

[19] The isotopic signatures in the first hundred meters are very different between the two stations (–2.7 ± 0.4 at GYR, –6.4 ± 0.4 and –6 ± 0.4 at EGY). These differences are consistent with the main origin of these surface waters (Figure 1a). Located east of the STF as clearly shown by the hydrographic parameters (Figure 2), EGY is under the influence of nonradiogenic waters flowing from the south. Contrastingly, surface waters found at GYR are ESPCW that flow in continuity with the western South Pacific Central Waters observed west of 115°W, although slightly fresher and colder. These waters have transited through the southwestern Pacific, following the anticyclonic subtropical gyre circulation. On their way, they might have changed their isotopic composition, when receiving inputs from the numerous volcanic (and radiogenic) islands occurring in this area *Grenier et al*. [2013].

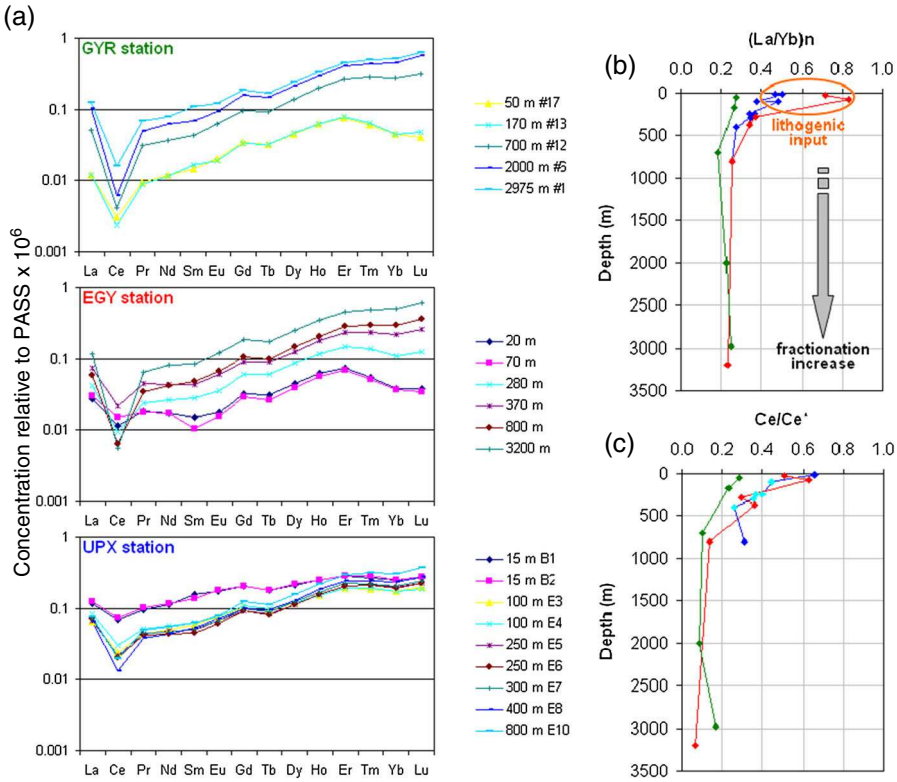

Figure 4. REE patterns normalized to PAAS at the different depths of the three stations. Figures 4b and 4c show the distributions of the normalized La/Yb ratio $(La/Yb)_N$ and of the Ce anomaly, calculated as $Ce/Ce^* = 2[Ce]_n/([La]_n + [Pr]_n)$ with depth.

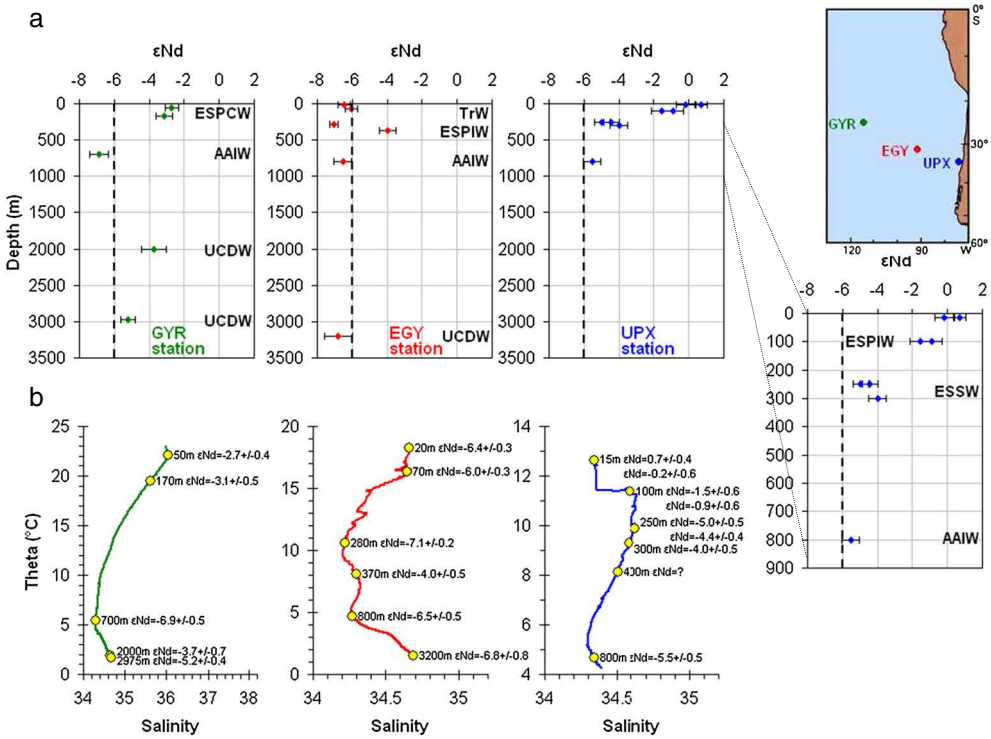

Figure 5. Vertical profiles of ε_{Nd} values at the three stations. An extended scale for the upper layers of station UPX is proposed. The dotted line marks the ε_{Nd} value of –6. Acronyms recall the water mass names.

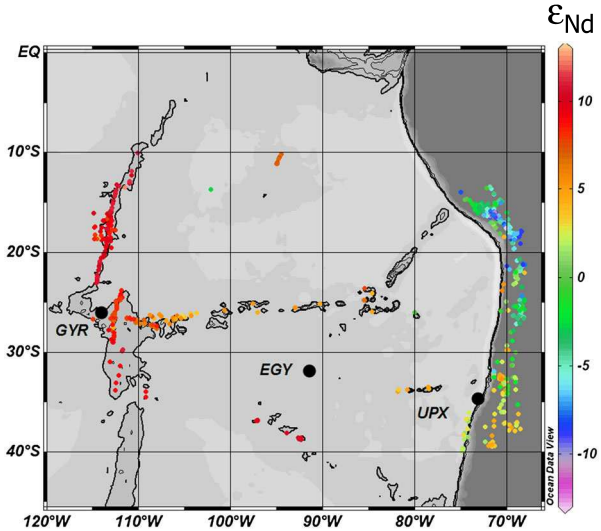

Figure 6. Map of the distribution of ε_{Nd} in the outcropping rocks and sediments at the surface of the continent and at the sea bottom. The radiogenic values close to station GYR are distributed along the East Pacific Rise, and the Easter-Salas y Gomez Seamount Chain in the east. Topographic lines are marking the depths of 3000 m, 2500 and 2000 m.

[20] Because GYR is located at the southeast border of the HSEA (Figure 1), the ε_{Nd} and REE concentrations measured at this station could be taken as characteristic of the waters originating from the southeast Pacific and feeding the thermocline of the south west Pacific [*Grenier et al.*, 2013]. However, we are aware of the scarcity of our data set. Thanks to the forthcoming GEOTRACES cruises, the set of data covering this area will considerably improve, confirming (or not) the hypotheses made here.

5.3. Ridge Exchange Above the East Pacific Rise

[21] Upper Circumpolar Deep Water (UCDW) has been identified at 3200 m at station EGY and at 2975 m and 2000 m at station GYR. ε_{Nd} values of these three samples are –6.8, –5.2, and –3.7, respectively. At this last station, AAIW displays a value of –6.9.

[22] Values around –6 are consistent with what we know for water masses of southern origin so far [*Lacan et al.*, 2012; *Carter et al.*, 2012; *Grasse et al.*, 2012; *Stichel et al.*, 2012]. More surprising is the radiogenic signal observed at 2000 m at station GYR. Hydrographic parameters of these three samples are exactly plotting along the same line, precluding that the UCDW might have undergone mixing with other water mass explaining the more radiogenic ε_{Nd} value. Northeast of our study area (14°S; 83°50′W, Figure 1a) but at the same depth, *Grasse et al.* [2012] identified very radiogenic North Pacific Deep Waters (NPDW; $\varepsilon_{Nd.} = -2.3 \pm 0.3$). However, these waters are slightly warmer (2.16°C) and lighter than our UCDW. In addition, *Reid* [1997] showed that waters found at 2000 m in our sampling area are flowing from the south whereas the area documented by *Grasse et al.* [2012] is affected by waters arriving from the North Pacific [see *Reid*, 1997; Figures 5 and 12a–12d]. These differences in hydrographical as well as dynamical properties likely explain the different isotopic signatures observed at comparable depths, NPDW being identified as an old water mass having circulated around the North Pacific before entering the eastern Equatorial Pacific (EEP; [*Grasse et al.*, 2012]).

[23] Station GYR is just located in the close vicinity of the intersection between the Easter Microplate West Rift in the west, the Easter-Salas y Gomez Seamount Chain in the east and the East Pacific Rise that extends north to south, a tectonically active area characterized by isotopic signatures ranging from 3 to 10 (Figure 6; [*Kingsley et al.*, 2007]). Besides, *Klinkhammer and Hudson* [1986] identified numerous hydrothermal plumes between 10°S and 40°S. These authors detected Mn maxima within a layer centered just below the depth of the observed radiogenic Nd value. We suggest here that this value might testify the local influence of these hydrothermal plumes, although the REE pattern of this radiogenic sample is not different from the two others. Because our samples are not filtered, potential influence of hydrothermal particles is not excluded. Transmissometer data were not collected under 1000 m during BIOSOPE, preventing any tracking of suspended particles. However, Nd concentration does not show any increase at this depth (Figure 3). On the contrary, Nd (and REE) concentrations are surprisingly low in these deep waters (<20 pmol/kg) compared to the remaining Pacific [*Lacan et al.*, 2012]. Such low values have also been observed in the deep waters of the EEP [*Grasse et al.*, 2012]. However, station GYR is very oligotrophic and remote enough not to undergo the influence of large particle fluxes, neither lithogenic or biogenic. It was even selected as the poorest-furthest station by the BIOSOPE PI [*Claustre et al.*, 2008]. Consequently, intense particle scavenging is not expected, contrasting to this extent with the EEP [*Grasse et al.*, 2012]. Here again, one cannot rule out a hydrothermal vent effect. Indeed, vent

fluids are injecting large amounts of dissolved and reduced Fe and Mn into the deep ocean. These elements are oxidized when entering in contact with seawater, yielding a "plume" of metalliferous particles that are known to remove by scavenging both the Nd brought by the vents and a significant fraction of the Nd contained in surrounding waters [*Michard et al*., 1983; *Piepgras and Wasserburg*, 1985; *German et al*., 1990]. Therefore, hydrothermal inputs have been considered as negligible for REE to the ocean so far and not taken into account in the models, neither as a source nor as a sink [*Jones et al*., 2008; *Siddall et al*., 2008; *Arsouze et al*., 2009; *Rempfer et al*., 2011]. Nevertheless, even if the net input flux is small (or negative), the gross one is loading very radiogenic dissolved Nd before its removal by scavenging in the hydrothermal plume, which could modify the water mass ε_{Nd} value in the vicinity of the ridge. Such "Ridge Exchange" would yield similar impact as the Boundary Exchange that occurs along the margins [*Lacan and Jeandel*, 2005; *Rickli et al*., 2011; *Carter et al*., 2012; *Grasse et al*., 2012]; changing the isotopic signature of the local water without increasing — even possibly decreasing—its Nd content. However, Ridge Exchange would result from a different process, dissolved radiogenic Nd being brought by the vent fluids and removed later by scavenging on Fe-Mn oxides. Contrastingly, Boundary Exchange is mostly attributed to release of Nd from solid margin sediments, followed by scavenging on particles (secondary phases precipitation or authigenic oxide formation). Therefore, whereas Nd removal is likely driven by close mechanisms in both Ridge and Boundary Exchanges, Nd inputs are not responding to the same process and source. We are aware of the fact that only one sample is driving this hypothesis and determining the volume of water impacted by this Ridge Exchange process is beyond the scope of this paper. However, better quantifying the contribution of this potential source to (i) the Nd isotopic signature and concentration distributions in the ocean and (ii) the oceanic cycle of each element, is of prime importance on the global scale. The future GEOTRACES Pacific sections GP16 and GP20 (www.geotraces.org) will provide the opportunity to document specifically the East Pacific Rise and its vicinity. This will allow constructing deep water element budgets as well as evaluating the impact of Ridge Exchange on them, which has not been possible here due to the scarcity of our data. Furthermore, modeling approaches as the one recently proposed for hydrothermal Fe could provide an efficient tool to evaluate the potential global impact of this source on the oceanic Nd isotope and REE budgets [*Tagliabue et al*., 2010].

6. Conclusions

[24] Three seawater profiles of Nd isotopes and REE concentrations provided new data on these parameters in the remote southeast Pacific and revealed that

- The coastal station UPX shows radiogenic Nd isotopic signature and flat REE patterns in surface waters, both suggesting a significant impact of element released from the sediments deposited on the Peru-Chile shelf and margin, confirming that Boundary Exchange processes are occurring along this coast.
- Exchange processes are also suspected close to the East Pacific Rise, in the deep waters of the GYR station. These exchanges might increase the Nd isotopic signature of the water mass—reflecting a gross input of Nd—perhaps depleting the REE concentrations, because of the rapid scavenging on Mn and Fe oxides known to occur in hydrothermal plumes. Estimating the broader impact of such Ridge Exchange process is envisaged by the forthcoming GEOTRACES cruises in this area.
- Nd and REE parameters of water masses not documented so far have been determined, as ESPIW ($\varepsilon_{Nd} \sim -1$ to -4) or ESSW ($\varepsilon_{Nd} \sim -4.5$). It also provided the REE concentrations and Nd isotopic signatures of subtropical water masses that are further advected westward and could be considered as sources of waters for the South West Pacific.

Acknowledgments

[25] The authors thank Hervé Claustre and Antoine Sciandra, respectively Principal Investigator and Chief Scientist of the BIOSOPE cruise for their offer to collect seawater at these three key-stations for Nd isotope and REE measurement purpose. Sophie Bonnet is also thanked for having kindly performed the collect. Frédéric Candaudap and Pierre Brunet are thanked for their technical help. Derek Vance is deeply thanked for welcoming us in Bristol in June 2010. The authors are also very grateful to the two anonymous reviewers and the Associate Editor Lou Derry who made very thorough and constructive comments. Roger François and Ester Garcia-Solsona are acknowledged for their helpful contributions. BIOSOPE project was supported by the INSU/LEFE program.

References

Akagi, T., F. F. Fu, Y. Hongo, and K. Takahashi (2011), Composition of rare earth elements in settling particles collected in the highly productive North Pacific Ocean and Bering Sea: Implications for siliceous-matter dissolution kinetics and formation of two REE-enriched phases, *Geochim. Cosmochim. Acta*, *75*, 4857–4876.

Arsouze, T., J. C. Dutay, F. Lacan, and C. Jeandel (2007), Modelling the neodymium isotopic composition with a global ocean circulation model, *Chem. Geol.*, *239*, 165–177.

Arsouze, T., J. C. Dutay, F. Lacan, and C. Jeandel (2009), Reconstructing the Nd oceanic cycle using a coupled dynamical - biogeochemical model, *Biogeosciences*, *6*, 2829–2846.

Bau, M., A. Koschinsky, P. Dulski, and J. R. Hein (1996), Comparison of the partitioning behaviours of yttrium, rare earth elements, and titanium between hydrogenetic marine ferromanganese crusts and seawater, *Geochim. Cosmochim. Acta*, *60*, 1709–1725.

Bertram, C. J., and H. Elderfield (1993), The geochemical balance of the rare earth elements and Nd isotopes in the oceans, *Geochim. Cosmochim. Acta*, *57*, 1957–1986.

Carter, P., D. Vance, C. D. Hillenbrand, J. A. Smith, and D. R. Shoosmith (2012), The neodymium isotopic composition of waters masses in the eastern Pacific sector of the Southern Ocean, *Geochim. Cosmochim. Acta*, *79*, 41–59.

Claustre, H., A. Sciandra, and D. Vaulot (2008), Introduction to the special section bio-optical and biogeochemical conditions in the South East Pacific in late 2004: the BIOSOPE program, *Biogeosciences*, *5*, 679–691.

Dahlqvist, R., P. S. Andersson, and J. Ingri (2005), The concentration and isotopic composition of diffusible Nd in fresh and marine waters, *Earth Planet. Sci. Lett.*, *233*, 9–16.

England, M. H., J. S. Godfrey, A. C. Hirst, and M. Tomczak (1993), The Mechanism for Antarctic Intermediate Water Renewal in a World Ocean Model, *J. Phys. Oceanogr.*, *23*, 1553–1560.

German, C. R., G. P. Klinkhammer, J. M. Edmond, A. Mitra, and H. Elderfield (1990), Hydrothermal Scavenging of Rare-Earth Elements in the Ocean, *Nature*, *345*, 516–518.

Goldstein, S., and S. R. Hemming (2003), Long Lived isotopic tracers in oceanography, paleoceanography and ice-sheet dynamics, *Treatise on Geochemistry*, 6.17, pp. 453–489, Elsevier, New-York.

Grasse, P., T. Stichel, R. Stumpf, L. Stramma, and M. Frank (2012), The distribution of neodymium isotopes and concentrations in the Eastern Equatorial Pacific: Water mass advection versus particle exchange., *Earth Planet. Sci. Lett.*, *353-354*, 198–207.

Grenier, M., C. Jeandel, F. Lacan, D. Vance, C. Venchiarutti, A. Cros, and S. Cravatte (2013), From the subtropics to the central equatorial Pacific Ocean: neodymium isotopic composition and rare earth element concentration variations *J. Geophys. Res.*, *118*, doi:10.1029/2012JC008239.

Jacobsen, S. B., and G. J. Wasserburg (1980), Sm-Nd isotopic evolution of chondrites, *Earth Planet. Sci. Lett.*, *50*, 139–155.

Jeandel, C. (1993), Concentration and isotopic composition of neodymium in the South Atlantic Ocean, *Earth Planet. Sci. Lett..*, *117*, 581–591.

Jeandel, C., T. Arsouze, F. Lacan, P. Techine, and J. C. Dutay (2007), Isotopic Nd compositions and concentrations of the lithogenic inputs into the ocean: A compilation, with an emphasis on the margins, *Chem. Geol.*, *239*, 156–164.

Jeandel, C., B. Peucker-Ehrenbrink, M. T. Jones, C. R. Pierce, E. H. Oelkers, Y. Godderis, F. Lacan, O. Aumont, and T. Arsouze (2011), Ocean Margins: The Missing Term in Oceanic Element Budgets?, *Eos Trans. AGU*, *92*, 217–224.

Jeandel, C., D. Thouron, and M. Fieux (1998), Concentrations and isotopic compositions of neodymium in the eastern Indian Ocean and Indonesian straits, *Geochim. Cosmochim. Acta*, *62*, 2597–2607.

Jones, K. M., S. P. Khatiwala, S. L. Goldstein, S. R. Hemming, and T. van de Flierdt (2008), Modeling the distribution of Nd isotopes in the oceans using an ocean general circulation model, *Earth Planet. Sci. Lett*, *272*, 610–619.

Kawabe, M., and S. Fujio (2010), Pacific Ocean Circulation Based on Observation, *J. Oceanogr.*, *66*, 389–403.

Kingsley, R. H., J. Blichert-Toft, D. Fontignie, and J. G. Schilling (2007), Hafnium, neodymium, and strontium isotope and parent-daughter element systematics in basalts from the plume-ridge interaction system of the Salas y Gomez Seamount Chain and Easter Microplate, *Geochem. Geophys. Geosyst.*, *8*, 1525–2027.

Klinkhammer, G., and A. Hudson (1986), Dispersal Patterns for Hydrothermal Plumes in the South-Pacific Using Manganese as a Tracer, *Earth Planet. Sci. Lett.*, *79*, 241–249.

Lacan, F., and C. Jeandel (2001), Tracing Papua New Guinea imprint on the central Equatorial Pacific Ocean using neodymium isotopic compositions and Rare Earth Element patterns, *Earth Planet. Sci. Lett.*, *186*, 497–512.

Lacan, F., and C. Jeandel (2005), Neodymium isotopes as a new tool for quantifying exchange fluxes at the continent-ocean interface, *Earth Planet. Sci. Lett.*, *232*, 245–257.

Lacan, F., K. Tachikawa, and C. Jeandel (2012), Neodymium isotopic composition of the oceans: a compilation of seawater data, *Chem. Geol.*, *300-301*, 177–184.

Landing, W. M., and K. W. Bruland (1987), The contrasting biogeochemistry of iron and manganese in the Pacific Ocean, *Geochim. Cosmochim Acta*, *51*, 29–43.

McLennan, S. M. (1989), Rare earth elements in sedimentary rocks: influence of provenance and sedimentary processes, Geochemistry and Mineralogy of Rare Earth Elements 169–200 pp., Mineralogical Society of America, Washington, D.C.

Michard, A., F. Albarède, G. Michard, J. F. Minster, and J. L. Charlou (1983), Rare-earth elements and uranium in high-temperature solutions from East Pacific Rise hydrothermal vent field (13°N), *Nature*, *303*, 795–797.

Moffet, J. W. (1990), Microbially cerium oxidation in seawater, *Nature*, *345*, 421–423.

Piepgras, D. J., and G. J. Wasserburg (1985), Strontium and neodymium isotopes in hot springs on the East Pacific Rise and Guaymas Basin, *Earth Planet. Sci. Lett.*, *72*, 341–356.

Piepgras, D. J., and G. J. Wasserburg (1987), Rare earth element transport in the western North Atlantic inferred from isotopic observations, *Geochim. Cosmochim. Acta*, *51*, 1257–1271.

Reid, J. L. (1997), On the total geostrophic circulation of the Pacific Ocean: flow patterns, tracers, and transports, *Prog. Oceanogr.*, *39*, 263–352.

Rempfer, J., T. F. Stocker, F. Joos, J. C. Dutay, and M. Siddall (2011), Modelling Nd-isotopes with a coarse resolution ocean circulation model: Sensitivities to model parameters and source/sink distributions, *Geochim. Cosmochim. Acta*, *75*, 5927–5950.

Rickli, J., M. Frank, A. R. Baker, S. Aciego, G. de Souza, R. B. Georg, and A. N. Halliday (2011), Hafnium and neodymium isotopes in surface waters of the eastern Atlantic Ocean: Implications for sources and inputs of trace metals to the ocean, *Geochim. Cosmochim. Acta*, *74*, 540–557.

Schneider, W., R. Fuenzalida, E. Rodriguez-Rubio, J. Garces-Vargas, and L. Bravo (2003), Characteristics and formation

of eastern South Pacific intermediate water, *Geophys. Res. Lett.*, *30*, doi:10.1029/2003GL017086.

Shabani, M. B., T. Akagi, and A. Masuda (1992), Preconcentration of trace rare-earth elements in seawater by complexation with bis(2-ethylhexyl)hydrogen phosphate and 2-ethylhexyl dihydrogen phosphate adsorbed on a C_{18} cartridge and determination by inductively coupled plasma mass spectrometry, *Anal. Chem.*, *64*, 737–743.

Siddall, M., S. Khatiwala, T. van de Flierdt, K. Jones, S. L. Goldstein, S. Hemming, and R. F. Anderson (2008), Towards explaining the Nd paradox using reversible scavenging in an ocean general circulation model, *Earth Planet. Sci. Lett.*, *274*, 448–461.

Silva, N., N. Rojas, and A. Fedele (2009), Water masses in the Humboldt Current System: Properties, distribution, and the nitrate deficit as a chemical water mass tracer for Equatorial Subsurface Water off Chile, *Deep-Sea Research Part II-Topical Studies in Oceanography*, *56*, 992–1008.

Sokolov, S., and S. Rintoul (2000), Circulation and water masses of the southwest Pacific: WOCE Section P11, Papua New Guinea to Tasmania, *J. Mar. Res.*, *58*, 223–268.

Stichel, T., M. Frank, J. Rickli, and B. A. Haley (2012), The hafnium and neodymium isotope composition of seawater in the Atlantic sector of the Southern Ocean, *Earth Planet. Sci. Lett.*, *317*, 282–294.

Tachikawa, K., C. Jeandel, and M. Roy-Barman (1999a), A new approach to the Nd residence time in the ocean: the role of atmospheric inputs, *Earth Planet. Sci. Lett.*, *170*, 433–446.

Tachikawa, K., C. Jeandel, A. Vangriesheim, and B. Dupre (1999b), Distribution of rare earth elements and neodymium isotopes in suspended particles of the tropical Atlantic Ocean (EUMELI site), *Deep-Sea Research Part I-Oceanographic Research Papers*, *46*, 733–755.

Tagliabue, A., L. Bopp, J. C. Dutay, A. R. Bowie, F. Chever, P. Jean-Baptiste, E. Bucciarelli, D. Lannuzel, T. Remenyi, G. Sarthou, O. Aumont, M. Gehlen, and C. Jeandel (2010), Hydrothermal contribution to the oceanic dissolved iron inventory, *Nature Geoscience*, *3*, 252–256.

Tomczak, M., and J. S. Godfrey (2003), Hydrology of the Pacific Ocean, Regional Oceanography: an Introduction, 2nd improved edition, pp. 137–156, Daya Publishing House, Delhi.

Tsuchiya, M., R. Lukas, R. Fine, E. Firing, and E. Lindstrom (1989), Source waters of the Pacific Equatorial Undercurrent., *Prog. Oceanogr.*, *23*, 101–147.

van de Flierdt, T., et al. (2012), GEOTRACES intercalibration of neodymium isotopes and rare earth element concentrations in seawater and suspended particles. Part 1: reproducibility of results for the international intercomparison, *Limnol. Oceanogr.*, *10*, 234–251.

Vance, D., and M. Thirlwall (2002), An assessment of mass discrimination in MC-ICPMS using Nd isotopes, *Chem. Geol.*, *185*, 227–240.

von Blanckenburg, F. (1999), Tracing Past Ocean Circulation?, *Science*, *286*, 1862b–1863.